2023 62nd IEEE Conference on Decision and Control (CDC)
December 13-15, 2023. Marina Bay Sands, Singapore

Formation control of differential-drive robots with input saturation and constraint on formation size

Ayush Agrawal[1], Mukunda Bharatheesha[2] and Shishir Kolathaya[3]

Abstract— **Cooperative control involves developing control strategies for individual robots that guarantee synchronized behavior of the states of all the robots in a team in some prescribed sense. This work presents a novel controller that achieves formation control for a group of differential-drive robots. First, we propose a nonlinear feedback control law that guarantees stable tracking of a reference trajectory for a single robot without exceeding the velocity limits of the robot. Using Lyapunov analysis, we obtain the necessary conditions on the control parameters and establish ultimate boundedness on error terms. Next, we formulate the formation control problem as a trajectory tracking problem for the multi-robot system and solve it using the proposed controller. Additionally, we provide constraints on formation size for a planned reference trajectory, ensuring smooth cornering of multi-robot formation without exceeding actuation limits.**

I. INTRODUCTION

Researchers in modern times recognize cooperative control as a potential solution to complex problems such as carrying heavy objects, search and rescue missions, and satellite clustering [11]. Formation control is considered a cooperative strategy for the positions and orientations of robots in a multi-robot system [4]. Formation control methods in the literature are broadly categorized under leader-follower methods [1], [3], virtual structure methods [4], [5], graph theory methods [6], [8]-[12], behavior-based methods [13], and artificial potential field based methods [14].

The authors in [1] proposed a controller for a single robot and leader-follower formation control to achieve trajectory tracking and collision avoidance (CA). However, the proposed controller fails to obey the actuation limit of the robots. Also, the stability condition presented in [1] is weak because it does not establish the boundedness of the error terms for time-varying trajectories. Unlike [1], where authors defined positions of followers using fixed distance and orientation relative to the leader, [2] uses curvilinear coordinates to determine the follower position relative to its assigned leader in the multi-vehicle system. Although this feature allows the formation to navigate flexibly on uneven terrains, the controller requires a finite segment of the leader's motion history to compute follower positions. A leader-follower formation control strategy with input saturation is given in [3]. The input constraints restrict the set of possible paths for the leader and the follower robots. The above methods are susceptible to single-point failure, i.e., the whole system will fail if communication with the leader is lost.

The virtual structure method solves this issue. The authors in [4] generate a virtual robot based on the formation structure and control its motion along the desired trajectory using backstepping and Lyapunov-based controllers. The controller ensures collision avoidance but fails to keep the speeds below practical limits. A hybrid approach is proposed in [5], where a Lyapunov-based controller controls the position of the virtual leader. The virtual leader's position is fed to a graph-theory-based position controller to control the offset between the followers. The control inputs are within the actuation limits; however, the convergence time is very large.

Instead of feeding the formation group trajectory to each robot, the pose information of neighboring robots is sufficient to achieve formation control. Researchers in [6], [8]-[12] utilized this idea and modeled the communication topology for a group of robots using the Laplacian matrix. In [6], the presence of root makes the system prone to single-point failure. Like [1], [5], formation generated in [6], [12] lacks the rotational degree of freedom. A synchronous approach to formation control is given in [7], [8]. In [7], synchronization error is specified for every pair of interacting agents, while in [8], it depends on the communication topology of the multi-robot system. The synchronization and tracking errors were asymptotically driven to zero using Lyapunov-based controllers in both [7], [8]. The algorithm in [7] ensures practical input magnitudes and algorithms in [8], [11] account for the effects of communication delay. However, none of these articles, including previously cited articles, discuss how large formation sizes can affect the kinematics of individual robots in a multi-robot formation.

Recent studies like in [15] propose an optimization-based solution to the trajectory tracking problem for a single robot. In [15], authors propose trajectory optimization and tracking control framework which guarantees the global exponential stability of the tracking errors. This open-loop control strategy relies on model accuracy. Hence, this strategy will lose efficacy if the system is subjected to unmodeled disturbances. This highlights the stature of closed-loop feedback control.

While contemplating these issues in formation control, we asked ourselves a question: *Can we design a closed-loop*

[1] Ayush Agarwal has received his Bachelor's degree from the Department of Mechanical Engineering at the Indian Institute of Technology Bombay, India. ayush.agrawal.c2021@iitbombay.org, aayush.agrawal149@gmail.com

[2]Mukunda Bharatheesha is a guest faculty at Robert Bosch Centre for Cyber-Physical Systems and a Senior Member of Technical Staff at ARTPARK, Indian Institute of Science, Bengaluru, India mukundab@iisc.ac.in, mukunda@artpark.in

[3]Shishir Kolathaya is an Assistant Professor at Robert Bosch Centre for Cyber-Physical Systems and the Department of Computer Science and Automation (CSA), Indian Institute of Science, Bengaluru, India shishirk@iisc.ac.in

This work is supported by the SERB Core Research Grant. No. CRG/2021/008115 and TCS Research

2023 62nd IEEE Conference on Decision and Control (CDC) | 979-8-3503-0124-3/23/$31.00 ©2023 IEEE | DOI: 10.1109/CDC49753.2023.10383912

feedback controller for differential drive robots such that they converge quickly to the desired time-varying trajectory while obeying their speed limits? Later, if the controller is extended for multi-robot formation control, can we maintain the stability of the formation in cornering maneuvers? If not, what are the limiting conditions?

We organize our work in the following sections to answer this question. In Section II, we design a controller that obeys input constraints and guarantees trajectory tracking. In Section III, we formulate the formation control problem as a trajectory tracking problem. We also discuss some constraints on the formation size for a given reference trajectory to avoid velocity limit violation in robots and ensure formation stability. In Section IV, we draw some conclusions and discuss some aspects of future work.

II. TRAJECTORY TRACKING CONTROLLER WITH INPUT CONSTRAINTS

We consider a differential-drive robot (see Fig.1) with wheels driven by identical motors. The wheel's radius is R, and the robot's track width is L. The instantaneous angular speed of the left and right wheels are denoted by ω_l and ω_r, respectively. The maximum limit on both motors' angular speed is $\omega_{r,\,l}^{max}$. In Fig.1, v denotes the linear velocity of the center of the axle, and ω denotes the angular velocity of the robot about the axis passing through the center of the axle (perpendicular to the plane of the paper). We can express $v,\ \omega$ as a function of $\omega_l,\ \omega_r$ as follows

$$\begin{bmatrix} v \\ \omega \end{bmatrix} = \begin{bmatrix} R/2 & R/2 \\ R/L & -R/L \end{bmatrix} \begin{bmatrix} \omega_r \\ \omega_l \end{bmatrix} \tag{1}$$

The kinematics of the differential-drive robot is governed by the following set of ordinary differential equations

$$\begin{aligned} \dot{x} &= \tfrac{R(\omega_r+\omega_l)}{2}\cos(\theta) = v\cos(\theta) \\ \dot{y} &= \tfrac{R(\omega_r+\omega_l)}{2}\sin(\theta) = v\sin(\theta) \\ \dot{\theta} &= \tfrac{R(\omega_r-\omega_l)}{L} \qquad\quad = \omega \end{aligned} \tag{2}$$

In (2), $[x,\ y,\ \theta]^T \in \mathbb{R}^3$ denotes the pose of the robot in a 2-D environment (see Fig.1). The robot has to follow a reference trajectory given by $(x_d(t),\ y_d(t))$ where $t \geq 0$ denotes time. Let $v_{max},\ \omega_{max}$ denote the maximum permissible values of $v,\ \omega$ respectively. Selecting [1]

$$v_{max} = \frac{R\omega_{r,\,l}^{max}}{2}, \quad \omega_{max} = \frac{R\omega_{r,\,l}^{max}}{L} \tag{3}$$

will ensure that $\omega_r,\ \omega_l$ never exceed $\omega_{r,\,l}^{max}$. Note that $v_{max},\ \omega_{max}$ are dependent on $\omega_{r,\,l}^{max}$ but the two quantities have different magnitudes.

Note 1: The reference trajectory is defined as the motion of a point whose coordinates at a particular time, $t \geq 0$, is given by $[x_d(t),\ y_d(t)]$. It is a time-varying trajectory. In principle, the robot has to chase a point whose coordinates $(x_d(t),\ y_d(t))$ are continuous functions of time, $t \geq 0$.

[1]Refer [18, I-A] to see how $v_{max},\ \omega_{max}$ are selected as in (3).

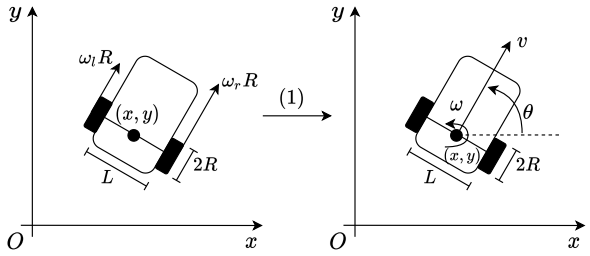

Fig. 1: Differential-drive kinematics: Transformation of control inputs from $[\omega_r,\ \omega_l]^T$ to $[v,\ \omega]^T$ using (1)

We define the position errors as, $e_x(t) = x_d(t) - x(t),\ e_y(t) = y_d(t) - y(t)$. We also define the desired orientation of the robot as follows:

$$\theta_d = \arctan 2(e_y,\ e_x)\big|_{unwrap}\ \forall\ (e_x, e_y) \in \mathbb{R}^2 - (0,0) \tag{4}$$

The discontinuous nature of the function - $\arctan 2(\cdot,\ \cdot)$ can cause disruptions in the robot's direction of motion. Hence for $(e_x,\ e_y) \neq (0,\ 0)$, we define the continuous form of θ_d in (4) using the *unwrap* function [17]. It should be noted that θ_d gives the instantaneous desired direction of motion for the robot at a time $t \geq 0$, that depends on the current position of the robot, $(x(t),\ y(t))$, and the current point on the reference trajectory, $(x_d(t),\ y_d(t))$. We define the orientation error as $e_\theta(t) = \theta_d(t) - \theta(t)$, see Fig. 2.

Some configurations might lead to a singular direction and impractically high magnitudes of linear and angular acceleration; see Fig.2. To avoid such cases, we assume throughout the paper that the reference trajectory has the following characteristics:

Assumption 1: The reference trajectory is smooth, i.e. both $x_d(t),\ y_d(t)$ are smooth function of time, $\forall\ t > 0$, and the first derivatives of $x_d(t),\ y_d(t)$, i.e., $\dot{x}_d(t),\ \dot{y}_d(t)$ are bounded. Moreover, the reference trajectory is such that it does not initiate sharp turns in the robot with respect to the current orientation of the robot, i.e.,

$$\cos(e_\theta) \in [-1,\ -\delta_\theta] \cup [\delta_\theta,\ 1] \tag{5}$$

for some $\delta_\theta \in (0, 1)$.

Note 2: The value of δ_θ corresponding to a given initial pose of the robot and a given reference trajectory is fixed and must lie in the interval $(0,\ 1)$.

Remark 1: Assumption 1 on the reference trajectory implies that scenarios shown in Fig.2 should be avoided.

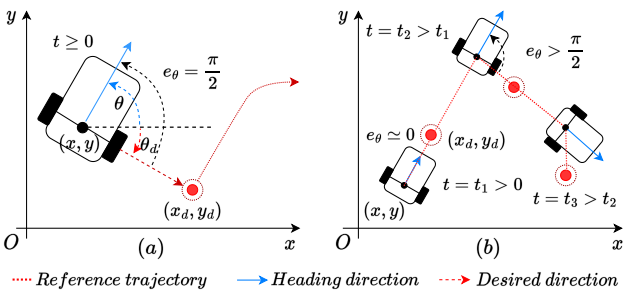

Fig. 2: (a) $e_\theta = \pi/2$, violation of non-holonomic constraint, (b) Sharp turn lead to sudden change in value of e_θ

1) In Fig.2(a), the robot cannot move along the desired direction of motion (singular direction, $e_\theta = \frac{\pi}{2}$) due to non-holonomic constraint.
2) In Fig.2(b), for the robot to keep following the reference trajectory on sharp turns at $t = t_2,\ t_3$, theoretically infinite angular acceleration (in motors) will be required.
3) The singularity condition $e_x = e_y = 0$ can be easily handled using zero controllers $v = \omega = 0$. It is improbable to experience this condition with real systems. Hence, we won't investigate this case further here.
4) The condition in (5) is not too restrictive since the robot can perform in-place rotation to reorient itself if the condition is not met.

Assumption 2: Define $\hat{\dot{\theta}}_d$ to be an estimate of $\dot{\theta}_d$ where,

$$\dot{\theta}_d = \frac{e_x\dot{e}_y - e_y\dot{e}_x}{D^2}, \quad D = \sqrt{e_x^2 + e_y^2} \tag{6}$$

At every time instant, we compute $\theta_d(t)$ using (4). With the value of $\theta_d(t)$ at the current and the previous time step, and using the backward difference method, we can estimate $\hat{\dot{\theta}}_d$ as follows

$$\hat{\dot{\theta}}_d(t) = \tfrac{\theta_d(t) - \theta_d(t-\tau)}{\tau} \tag{7}$$

where $\tau \in (0,\ 1)$ represents simulation time step. The estimation error in $e_x(t),\ e_y(t)$ (estimated using odometry) will propogate while computing $\hat{\dot{\theta}}_d(t)$. Hence, there exists an estimation error in $\hat{\dot{\theta}}_d(t)$ relative to $\dot{\theta}_d$. We denote the error by a small positive number, ϵ_θ, as follows

$$|\hat{\dot{\theta}}_d - \dot{\theta}_d| \leq \epsilon_\theta = \Omega(\tau)^2, \quad \epsilon_\theta \in \mathbb{R}_{>0} \tag{8}$$

In a practical setting, the value of ϵ_θ depends on the sensor resolution, the robot's specification, and the reference trajectory.

Assumption 3: The maximum translational speed of robot, v_{max} is much greater than $|v_{traj}^{sup}| = \sup_{t\geq 0} \sqrt{\dot{x}_d^2 + \dot{y}_d^2}$ s.t.

$$\frac{v_{max}\delta_\theta^2}{|v_{traj}^{sup}|} > 1 \tag{9}$$

for a given $\delta_\theta \in (0,\ 1)$.

Remark 2: Condition (9) is also not restrictive. Planning a reference trajectory such that $|v_{traj}^{sup}| < v_{max}$ will satisfy the practical requirement for the robot to be faster than the reference trajectory it should track.

The robot will approach the reference trajectory, and stable tracking will be achieved if $e_x,\ e_y,\ e_\theta$ converge to a neighborhood close to the origin in finite time such that,

$$\|e_x,\ e_y\|_2 = D(t) \leq b_D, \quad |e_\theta(t)| \leq b_{e_\theta} \quad \forall\ t \geq T \tag{10}$$

for some small positive number $b_D,\ b_{e_\theta} > 0$.

Note 3: $\dot{\theta}_d$ can be estimated more accurately using sophisticated methods other than the backward difference method. However, a more accurate estimation of $\dot{\theta}_d$ won't profoundly change the values of ultimate bounds b_{e_θ} in (27). Refer [18, I-D] for more discussion in this regard.

[2]Theoretical explanation for $\epsilon_\theta = \Omega(\tau)$ in (8) is provided in [18, I-B].

Theorem 1. *Consider a robot whose kinematics is defined as in (2) and has a maximum linear and angular speed as $v_{max},\ \omega_{max} > 0$ respectively (3). The reference trajectory is described as $(x_d(t),\ y_d(t))$ that satisfies assumptions 1, 2, and 3. Then, stable tracking (10) is guaranteed without exceeding actuator limits if the following closed-loop negative feedback controller is applied,*

$$v = v_{max}\cos(e_\theta)\frac{\eta_v D}{1 + \eta_v D} \tag{11}$$

$$\omega = (\omega_{max} - \Omega_{max})\tanh(\eta_\omega e_\theta) + \hat{\dot{\theta}}_d \tag{12}$$

for $D = \sqrt{e_x^2 + e_y^2}$ and positive constants $\eta_v,\ \eta_\omega,\ \Omega_{max} > 0$. The choice of $\Omega_{max},\ \eta_v$ satisfy

$$\eta_v < \frac{2(\omega_{max} - 2\epsilon_\theta)}{3v_{max}} \tag{13}$$

$$\Omega_{max} < \omega_{max} - \epsilon_\theta \tag{14}$$

Further, $|\hat{\dot{\theta}}_d|$ is bounded $\forall\ t \geq 0$ thereby adhering to actuation limits of the robot.

Proof. With linear and angular velocity (v, ω) as the control input in the kinematic model (2) of differential drive robot, we write the error dynamics as follows

$$\begin{aligned}
\dot{e}_x &= \dot{x}_d - v\cos(\theta) \\
&= \dot{x}_d - v(\cos(e_\theta)\cos(\theta_d) + \sin(e_\theta)\sin(\theta_d)) \\
\dot{e}_y &= \dot{y}_d - v\sin(\theta) \\
&= \dot{y}_d - v(\sin(e_\theta)\cos(\theta_d) - \cos(e_\theta)\sin(\theta_d)) \\
\dot{e}_\theta &= \dot{\theta}_d - \omega
\end{aligned} \tag{15}$$

Using the expressions $\cos(\theta_d) = \frac{e_x}{D}$ and $\sin(\theta_d) = \frac{e_y}{D}$ and applying the controller (11)-(12) we obtain

$$\begin{aligned}
\dot{e}_x &= \dot{x}_d - v_{max}\frac{\eta_v}{1 + \eta_v D}(e_x\cos^2(e_\theta) + e_y\cos(e_\theta)\sin(e_\theta)) \\
\dot{e}_y &= \dot{y}_d - v_{max}\frac{\eta_v}{1 + \eta_v D}(e_y\cos^2(e_\theta) - e_x\cos(e_\theta)\sin(e_\theta)) \\
\dot{e}_\theta &= \dot{\theta}_d - (\omega_{max} - \Omega_{max})\tanh(\eta_v e_\theta) - \hat{\dot{\theta}}_d
\end{aligned} \tag{16}$$

II-A. Lyapunov Analysis

We prove that the system (2) is ultimately bounded for the proposed controller (11), (12) using *Theorem 4.18* of [16]. In this analysis, we constructed the Lyapunov candidate functions separately for $D(t)$ & $e_\theta(t)$ and eventually established boundedness for the entire system. A small positive constant[3] $0 < \zeta \ll 1$ is chosen to define upper and lower bounds for the Lyapunov functions chosen for $D,\ e_\theta$, see (17), (23).

For Lyapunov analysis of $D(t)$, we choose the Lyapunov candidate function $V_D : [0, \infty) \times \mathbb{R}^2 \to \mathbb{R}$ as follows

$$\alpha_1(D) = \frac{D^2}{2 + \zeta} \leq V_D(D) = \frac{D^2}{2} \leq \alpha_2(D) = \frac{D^2}{2 - \zeta} \tag{17}$$

[3][18, I-D] outlines the role of ζ in finding the ultimate bounds on $D,\ e_\theta$.

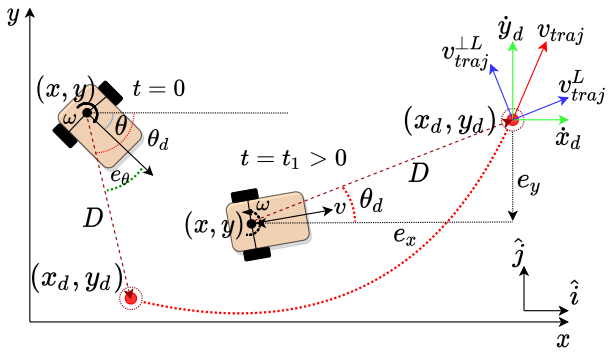

Fig. 3: Cartesian components of v_{traj} (Green): $(\dot{x_d}, \dot{y_d})$, Components of v_{traj} along and $\perp$ to L (Blue): $(v^L_{traj}, v^{\perp L}_{traj})$. D denotes the distance between $(x,\ y)$ and $(x_d,\ y_d)$

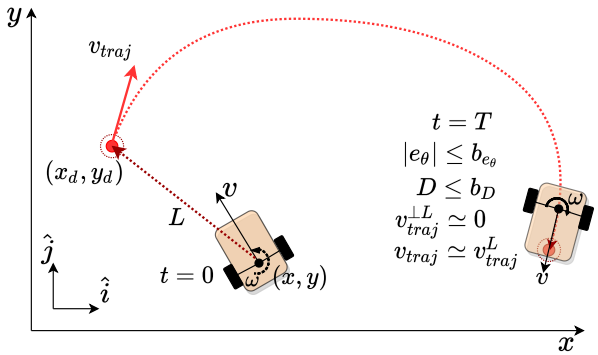

Fig. 4: Stable tracking achieved by differential drive robot using controller (11), (12)

Here $\alpha_1, \alpha_2, V_D \in \kappa_\infty$ class of function. Then, the derivative of V_D along the trajectories of the error dynamics is

$$\dot{V}_D = D\dot{D} = e_x\dot{e_x} + e_y\dot{e_y}$$
$$\dot{V}_D = \dot{x}_d e_x + \dot{y}_d e_y - \frac{\eta_v v_{max}\cos^2(e_\theta)(e_x^2 + e_y^2)}{1 + \eta_v D} \quad (18)$$

We define instantaneous velocity of desired trajectory as $v_{traj} = \dot{x}_d\hat{i} + \dot{y}_d\hat{j}$, $|v_{traj}| = \sqrt{\dot{x}_d^2 + \dot{y}_d^2}$ ($\hat{i}$, $\hat{j}$ represent unit vector along x and y direction). Let the line joining the current position of robot, $(x(t),\ y(t))$, and the current reference point, $(x_d(t),\ y_d(t))$, be called L. The component of v_{traj} along L is denoted by $v^L_{traj} = \dot{x}_d\cos(\theta_d) + \dot{y}_d\sin(\theta_d)$, and the perpendicular component $v^{\perp L}_{traj} = \dot{y}_d\cos(\theta_d) - \dot{x}_d\sin(\theta_d)$, see Fig.3. Multiplying v^L_{traj}, $v^{\perp L}_{traj}$ with D, we get $Dv^L_{traj}(t) = \dot{x}_d e_x + \dot{y}_d e_y$ and $Dv^{\perp L}_{traj}(t) = \dot{y}_d e_x - \dot{x}_d e_y$.

$$\dot{V}_D \leq -\left(\frac{v_{max}\delta_\theta^2\eta_v D}{1+\eta_v D} - v^L_{traj}\right)D \leq -\left(\frac{v_{max}\delta_\theta^2\eta_v D}{1+\eta_v D} - |v^{sup}_{traj}|\right)D \quad (19)$$

For $D \geq \mu_D = (1+\zeta)\frac{|v^{sup}_{traj}|}{\eta_v\left(v_{max}\delta_\theta^2 - |v^{sup}_{traj}|\right)} > 0$,

$$\dot{V}_D \leq -\zeta|v^{sup}_{traj}|\left(\frac{v_{max}\delta_\theta^2 - |v^{sup}_{traj}|}{v_{max}\delta_\theta^2 + |v^{sup}_{traj}|}\right)D = -W(D) \leq -W(\mu_D) \quad (20)$$

Note that $W(D)$ is a continuous positive definite function. Hence, the result of *Theorem 4.18* of [16] will hold for any initial state $(e_x(0),\ e_y(0))$.

$$\|e_x, e_y\|_2 = D(t) \leq \alpha_1^{-1}(\alpha_2(\mu_D)) \quad \forall\ t \geq T_D$$
$$D(t) \leq \frac{\sqrt{2+\zeta}}{\sqrt{2-\zeta}}\mu_D = b_D \quad \forall\ t \geq T_D \quad (21)$$

The value of T_D in (21) is determined as follows

$$\dot{V}_D \leq -W(\mu_D) \implies \int_0^t \dot{V}_D \leq \int_0^t -W(\mu_D)$$
$$V_D(t) - V_D(0) \leq -W(\mu_D)t \implies V_D(t) \leq V_D(0) - W(\mu_D)t$$

This shows that $V_D(D(t))$ reduces to $V_D(b_D)$ within the time interval of $[0, T_D]$ where,

$$T_D = \frac{V_D(D(0)) - V_D(b_D)}{W(\mu_D)} \quad (22)$$

Unlike D, $e_\theta \in [-\cos^{-1}(\delta_\theta), \cos^{-1}(\delta_\theta)] \subseteq (-\pi/2, \pi/2)$. For e_θ, we choose the Lyapunov function candidate $V_{e_\theta} : [0,\infty) \times [-\cos^{-1}(\delta_\theta), \cos^{-1}(\delta_\theta)] \to \mathbb{R}$ as follows

$$\alpha_3(e_\theta) = \frac{e_\theta^2}{2+\zeta} \leq V_{e_\theta}(e_\theta) = \frac{e_\theta^2}{2} \leq \alpha_4(e_\theta) = \frac{e_\theta^2}{2-\zeta} \quad (23)$$

The derivative of V_{e_θ} along the trajectories of $e_\theta(t)$ is

$$\dot{V}_{e_\theta} = e_\theta(\dot{\theta}_d - \hat{\dot{\theta}}_d) - (\omega_{max} - \Omega_{max})\tanh(\eta_\omega e_\theta)e_\theta \quad (24)$$

$$\dot{V}_{e_\theta} \leq -\big((\omega_{max} - \Omega_{max})|\tanh(\eta_\omega e_\theta)| - \epsilon_\theta\big)|e_\theta| \quad (25)$$

For $|e_\theta| \geq \mu_{e_\theta} = \frac{(1+\zeta)}{2\eta_\omega}\ln\left(\frac{\omega_{max}-\Omega_{max}+\epsilon_\theta}{\omega_{max}-\Omega_{max}-\epsilon_\theta}\right) > 0$

$$\dot{V}_{e_\theta} \leq -\left((\omega_{max} - \Omega_{max})\tanh(\eta_\omega\mu_\theta) - \epsilon_\theta\right)|e_\theta| = -U(e_\theta)$$
$$\dot{V}_{e_\theta} \leq -U(e_\theta) \leq -U(\mu_{e_\theta}) \quad (26)$$

Note 4: μ_{e_θ} is strictly positive if $(\omega_{max} - \Omega_{max} - \epsilon_\theta) > 0$. Condition in (14) obtained.

V_{e_θ}, α_3, $\alpha_4 \in \kappa$ class of functions and $U(e_\theta)$ is a continuous positive definite function in the domain of e_θ. To apply *Theorem 4.18* of [16] in this case, we choose $r = \cos^{-1}\delta_\theta - \zeta > 0$. We find the value of $\alpha_4^{-1}(\alpha_3(r)) = \sqrt{\frac{2-\zeta}{2+\zeta}}r$. Choosing sufficiently large positive value for η_ω will ensure $\mu_{e_\theta} < \alpha_4^{-1}(\alpha_3(r))$. By *Theorem 4.18* of [16], for every initial state $|e_\theta(0)| \leq \alpha_4^{-1}(\alpha_3(r))\ \exists\ T_{e_\theta} \geq 0$ s.t.

$$|e_\theta(t)| \leq \alpha_3^{-1}(\alpha_4(\mu_{e_\theta})) = \frac{\sqrt{2+\zeta}}{\sqrt{2-\zeta}}\mu_{e_\theta} = b_{e_\theta}\ \forall\ t \geq T_{e_\theta} \quad (27)$$

$V_{e_\theta}(e_\theta(t))$ reduces to $V_{e_\theta}(b_{e_\theta})$ within the time interval of $[0, T_{e_\theta}]$ where, T_{e_θ} can be computed in the same way as T_D.

$$T_{e_\theta} = \frac{V_{e_\theta}(e_\theta(0)) - V_{e_\theta}(b_{e_\theta})}{U(\mu_{e_\theta})} \quad (28)$$

By *Definition 4.6* of [16], $D(t)$ is globally uniformly ultimately bounded by b_D and $e_\theta(t)$ is uniformly ultimately bounded by $b_{e_\theta}\ \forall\ t \geq T = \max\{T_D, T_{e_\theta}\}$.

II-B. Upper bound of $|\hat{\dot{\theta}}_d|$

We begin by obtaining an upper bound on $\dot{\theta}_d$ by starting with (6). Substituting (15), (16) in (6)

$$\left|\dot{\theta}_d\right| = \left|\frac{e_x\dot{e}_y - e_y\dot{e}_x}{D^2}\right| = \left|\frac{-Dv_{max}\sin(2e_\theta)\frac{\eta_v D}{2(1+\eta_v D)} + D(v_{traj}^{\perp L})}{D^2}\right|$$
$$\leq \left|\frac{v_{max}\eta_v}{2(1+\eta_v D)}\right| + \frac{|v_{traj}^{\perp L}|}{D} \leq \left|\frac{v_{max}\eta_v}{2(1+\eta_v D)}\right| + \frac{|v_{traj}^{sup}|}{D} \tag{29}$$

In the region outside the ultimate bound: $D(t) \geq b_D$. Also,

$$b_D > \mu_D > \frac{|v_{traj}^{sup}|}{\eta_v\left(v_{max}\delta_\theta^2 - |v_{traj}^{sup}|\right)} \geq \frac{|v_{traj}^{sup}|}{\eta_v\left(v_{max} - |v_{traj}^{sup}|\right)} \tag{30}$$

Therefore, by substituting the result of (30) in (29)

$$|\dot{\theta}_d| < \left|\frac{\eta_v(v_{max} - |v_{traj}^{sup}|)}{2}\right| + \eta_v(v_{max} - |v_{traj}^{sup}|)$$
$$|\dot{\theta}_d| < \frac{3\eta_v v_{max}}{2} \tag{31}$$

Now, using (8) and upper bound on $|\dot{\theta}_d|$ in (31), we get

$$|\hat{\dot{\theta}}_d| \leq |\dot{\theta}_d| + \epsilon_\theta \implies |\hat{\dot{\theta}}_d| < \frac{3\eta_v v_{max}}{2} + \epsilon_\theta \tag{32}$$

If we choose η_v as per (13), then choosing $\Omega_{max} = \frac{3\eta_v v_{max}}{2} + \epsilon_\theta$ will satisfy (14). This way we have proved that $|\hat{\dot{\theta}}_d|$ is upper bounded for $D(t) \geq b_D$. Even if $D(t)$ goes arbitrarily close to zero, $|\hat{\dot{\theta}}_d|$ will remain upper bounded because

$$\lim_{D\to 0} \frac{|v_{traj}^{\perp L}|}{D} = 0 \tag{33}$$

A detailed proof of (32) and (33) is given in [18, I-C].

From the results of II-A, II-B, we conclude that stable tracking as defined in (10) is guaranteed without exceeding actuator limits. □

II-C. Simulation Example

Example 1: To illustrate the results of Theorem 1, simulations were performed in MATLAB/Simulink. We applied the proposed controller in (11), (12) to an in-built Simulink model for differential-drive kinematics, see [18, Fig.3]. Time integration in the model was performed using the *ode*45 solver with a step size of $\tau = 0.01$ seconds.

In this example, initial pose of the robot is $[x(0),\ y(0),\ \theta(0)]^T = [0,\ -1,\ 0.5]^T$. Simulation time is set to $T_{sim} = 200$ seconds and the robot is required to track an elliptical trajectory $[x_d(t),\ y_d(t)] = \left[10\cos\left(\frac{2\pi t}{T_{sim}}\right),\ 6\sin\left(\frac{2\pi t}{T_{sim}}\right)\right]$ until the end of simulation time. Chosen control parameters are listed in Table I.

Controller parameters			
Parameter	Value	Parameter	Value
R	$0.02m$	η_v	10
L	$0.09m$	η_ω	10
$\omega_{r,\,l}^{max}$	$52^{rad}/_{s}$	τ	0.01
v_{max}	$0.52\ ^{m}/_{s}$	ϵ_θ	$0.1^{rad}/_{s}$
ω_{max}	$11.5^{rad}/_{s}$	Ω_{max}	$7.9^{rad}/_{s}$

TABLE I

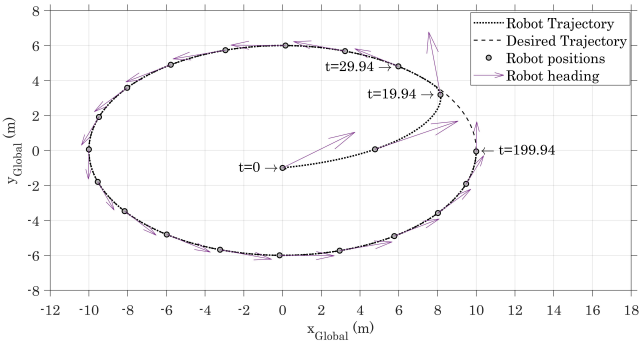

Fig. 5: Differential drive robot tracking elliptical trajectory using proposed controller (11), (12)

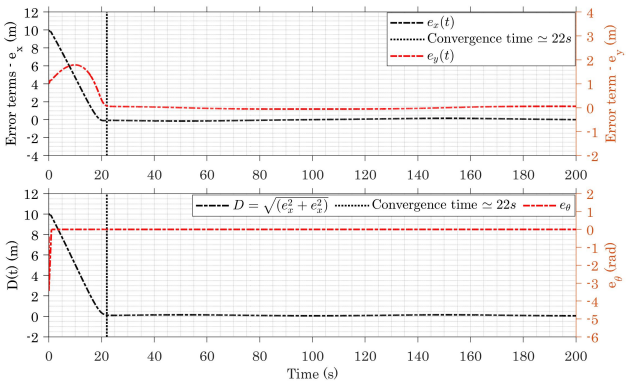

Fig. 6: Error terms - e_x, e_y, D, e_θ converging to neighbourhood around zero.

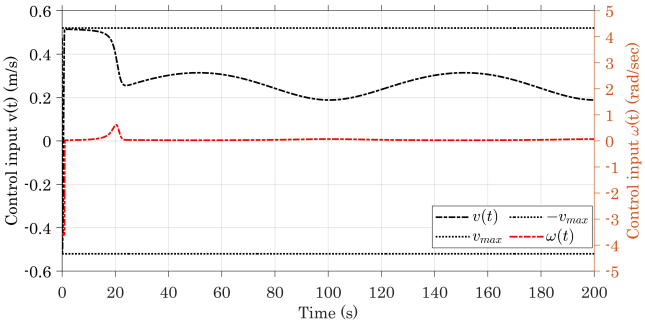

Fig. 7: Control inputs $v(t)$, $\omega(t)$ and their saturation limits

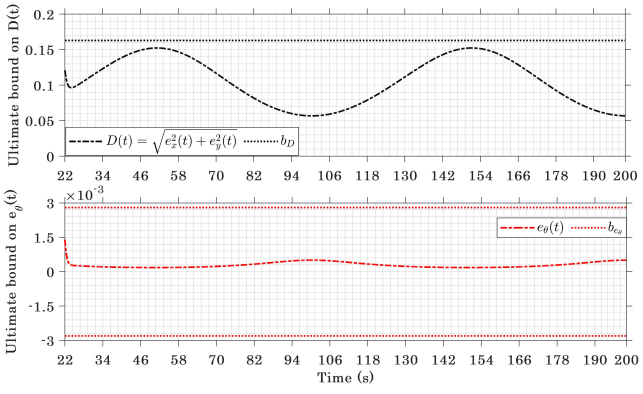

Fig. 8: $D(t)$, $e_\theta(t)$ ultimately bounded by b_D, b_{e_θ} respectively, for $t > 22s$

For $\zeta = 0.01$, we get $b_D = 0.163m$, and $b_{e_\theta} = 2.8 \times 10^{-3} rad$. It must be noted that the value of $b_D = 0.163m$ is 0.815% of the length of the major axis of the elliptical trajectory. Higher peak angular speed of motors will yield even lower values of $b_D,\ b_{e_\theta}$. The upper bound b_D on $D(t)$ can be reduced further by reducing the value of $|v_{traj}^{sup}|$.

Fig.5, Fig.6 shows the robot approaching the reference trajectory. The variation of control input $v(t), \omega(t)$ for $t \in [0,\ T_{sim}]$ is shown in Fig.7. It must be noted that $v(t),\ \omega(t)$ does not exceed $v_{max} = 0.52\frac{m}{s},\ \omega_{max} = 11.5\frac{rad}{s}$ respectively. Fig.8 highlights the convergence of $D,\ |e_\theta|$ to values within their respective ultimate bounds $b_D,\ b_{e_\theta}$.

III. FORMATION CONTROL AND CONSTRAINT ON RADIUS OF FORMATION

In this section, we study the problem of formation control for a multi-robot system composed of N differential drive robots. The kinematic model of the robots with linear and angular velocity as control inputs is described by

$$\begin{aligned} \dot{x}_i &= v_i \cos(\theta_i), & x_i(0) &= x_i^0 \\ \dot{y}_i &= v_i \sin(\theta_i), & y_i(0) &= y_i^0 \\ \dot{\theta}_i &= \omega_i, & \theta_i(0) &= \theta_i^0 \end{aligned} \tag{34}$$

where $[x_i, y_i, \theta_i]^T \in \mathbb{R}^3$ denotes the pose, and $v_i,\ \omega_i$ are linear & angular velocity of i^{th} robot respectively, $i \in \{1, 2, ...N\}$. We define the formation control problem as follows.

Problem 2: Given a desired formation for a group of N differential-drive robots and a reference trajectory, $[x_d(t),\ y_d(t)]$ for the center of formation. The objective for the robots is to converge to a stable formation around the center such that the center tracks the given desired trajectory, and robots maintain the formation under set actuation limits. The controller must be implemented locally on each robot to achieve the aforementioned task of formation control.

As mentioned in Section I, we address the formation control problem using the virtual-structure approach, where we consider a virtual leader to generate the desired formation. We assign '0' as the index of the virtual leader. The desired position of follower robots is defined relative to the virtual leader using polar coordinates to create the desired formation shape; see Fig.9(a). It is possible to produce any formation shape by assigning appropriate polar coordinates to the follower robots.

We particularly consider the circular formation and analyze the effects of its size on the kinematics of follower robots. We denote the formation radius by R_f. Each robot in the formation can access the instantaneous global pose of the virtual leader, $[x_0, y_0, \theta_0]^T$, see Fig.9(b).

At a particular instance of time, say $t \geq 0$, let $B_i^{des} = [x_i^{G.des}, y_i^{G.des}]^T$ be the desired global position of the i^{th} robot in the formation, and $b_i^{des} = [x_i^{l.des}, y_i^{l.des}]^T$ be its desired local position with respect to the coordinate system attached to the virtual leader $\forall\ i \in \{1, 2, ..., N\}$. The desired local position of the i^{th} robot (b_i^{des}) relative to the virtual leader is defined using polar coordinates, (R_f, α_i), see Fig.9(a).

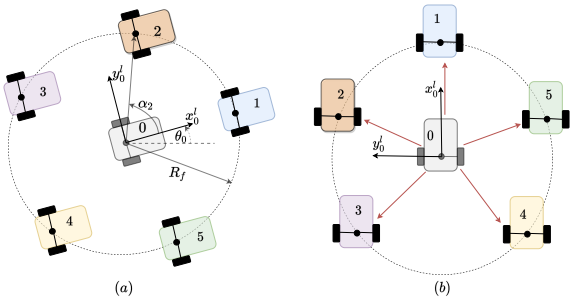

Fig. 9: (a) Circular arrangement of follower robots relative to the virtual leader using polar coordinates $(R_f,\ \alpha_i)\ \forall\ i \in \{0, 1, ..., N\}$, (b) All followers receive instantaneous global pose of virtual leader, $[x_0,\ y_0,\ \theta_0]^T$

$$b_i^{des} = \begin{bmatrix} x_i^{l.des} \\ y_i^{l.des} \end{bmatrix} = \begin{bmatrix} R_f \cos(\alpha_i) \\ R_f \sin(\alpha_i) \end{bmatrix} \tag{35}$$

$$B_i^{des} = \begin{bmatrix} x_i^{G.des} \\ y_i^{G.des} \end{bmatrix} = \begin{bmatrix} x_0 \\ y_0 \end{bmatrix} + \begin{bmatrix} R_f \cos(\theta_0 + \alpha_i) \\ R_f \sin(\theta_0 + \alpha_i) \end{bmatrix} \tag{36}$$

Here, $[x_0, y_0, \theta_0] \in \mathbb{R}^3$ is the pose of the virtual leader. While defining the desired global position of followers in (36), the orientation of the virtual leader is taken into account to allow the entire formation to align itself with the orientation of the virtual leader, see Fig.9(a). Unlike [1], [5], [6], [12], (36) ensures the formation has a rotational degree of freedom. Construction of circular formation using (35), (36) ensures that the virtual leader will coincide with the center of the formation circle (not the centroid of robots' positions) after achieving the formation. Hence, we assign the reference trajectory, $[x_d(t),\ y_d(t)]$ to the virtual leader.

We aim to allow robots to converge to a stable circular formation such that the center of formation (coinciding with the virtual leader) tracks the given reference trajectory, $(x_d(t),\ y_d(t))$. This will be guaranteed if the error terms $e_{x_i},\ e_{y_i},\ e_{\theta_i}\ \forall\ i \in \{0, 1, 2, ..., N\}$ converge to a neighborhood close to the origin in finite time such that,

$$\begin{aligned} \sqrt{e_{x_i}(t)^2 + e_{y_i}(t)^2} = D_i(t) &\leq b_{D_i}\ \forall\ t \geq T_f \\ |e_{\theta_i}(t)| &\leq b_{e_{\theta_i}}\ \forall\ t \geq T_f \end{aligned} \tag{37}$$

for small positive numbers $b_{D_i},\ b_{e_{\theta_i}} > 0\ \forall\ i \in \{0, 1, ...N\}$.

Assumption 4: The formation radius R_f is strictly less than the minimum radius of curvature of the reference trajectory $[x_d(t),\ y_d(t)]$ for the center of formation circle, i.e.,

$$R_f < R_{des}^{min} = \underset{t>0}{\operatorname{argmin}} \left| \frac{(\dot{y}_d^2 + \dot{x}_d^2)^{1.5}}{\dot{x}_d \ddot{y}_d - \dot{y}_d \ddot{x}_d} \right| \tag{38}$$

and the choice of R_f as per (38) must also satisfy the following condition

$$|v_{traj}^{sup}| \left(1 + \frac{R_f}{R_{des}^{min}}\right) < v_{max} \tag{39}$$

where $|v_{traj}^{sup}| = \sup_{t \geq 0} \sqrt{\dot{x}_d^2 + \dot{y}_d^2}$.

Remark 3: Assumption 4 imposes the following conditions on the size of formation for a given reference trajectory.

1) Planned formation size must satisfy (38). If not, then the reference trajectory for the robot closest to the curvature center of $[x_d(t),\ y_d(t)]$ will not be smooth and will result in violation of assumption 1, leading to high angular velocities in robot (see Example 3 of III-B)
2) In addition to (38), the chosen value of R_f must also satisfy (39). The robot farthest from the curvature center of $[x_d(t),\ y_d(t)]$ has to travel faster than other followers to keep the formation intact; hence (39) must hold.
3) (38), (39) are essential for planning formations in a given scenario. These constraints are not explicit parts of the controller, but disobeying them will result in failure of formation due to the above two listed reasons.
4) Finding a similar condition for non-circular formation requires a meticulous analysis of each robot's dynamics in formation. We will consider this in our future work.

Theorem 2. *Given a group of N differential drive robots whose kinematics are defined by (34). The maximum linear and angular speed of the robots are $v_{max},\ \omega_{max} > 0$ respectively (3). Also, given a reference trajectory $[x_d(t),\ y_d(t)]$ for the formation center which satisfies assumptions $1-3$. The formation radius R_f is chosen such that (38), (39) holds. Then the robots will converge to a stable formation (37) around the virtual leader if the following controller is applied $\forall\ i \in \{0, 1, 2, ..., N\}$*

$$v_i = v_{max}\cos(e_{\theta_i})\frac{\eta_v D_i}{1+\eta_v D_i} \tag{40}$$

$$\omega_i = (\omega_{max} - \Omega_{max})\tanh(\eta_\omega e_{\theta_i}) + \hat{\dot{\theta}}_{d_i} \tag{41}$$

for $D_i = \sqrt{e_{x_i}^2 + e_{y_i}^2}$ and positive constants $\eta_v,\ \eta_\omega,\ \Omega_{max} > 0$. The choice of η_v and Ω_{max} must satisfy (13), (14).

Proof. Consider the error dynamics of the robots in (15) $\forall\ i \in \{1, 2, 3..., N\}$. Using the expressions $\cos(\theta_{d_i}) = \frac{e_{x_i}}{D_i}$ and $\sin(\theta_{d_i}) = \frac{e_{y_i}}{D_i}$ and applying the controller (40), (41) to (15), we obtain the error dynamics in (16) $\forall\ i \in \{0, 1, ..., N\}$. As discussed previously, the virtual leader is required to track the given reference trajectory $[x_d(t),\ y_d(t)]$.

III-A. Lyapunov Analysis

Details of this analysis are presented in [18, Sec. II-A] □

III-B. Simulation Examples

Example 2: To illustrate the results of Theorem 2 simulations were performed in MATLAB/Simulink. We implemented the proposed controller in (40), (41) to a group of $N = 5$ differential drive robots in Simulink. The virtual leader is modeled using (34) in Simulink. The robots have to converge to a regular pentagon-like formation circumscribed by a circle of radius $R_f = 2m$ with the virtual leader at its center. By assumption 4, we choose $R_{min}^{des} = 10m$ and $|v_{traj}^{sup}| = \frac{\pi}{10} m/s$. The rest of the control parameters are the same as given in Table I. Based on the chosen values,

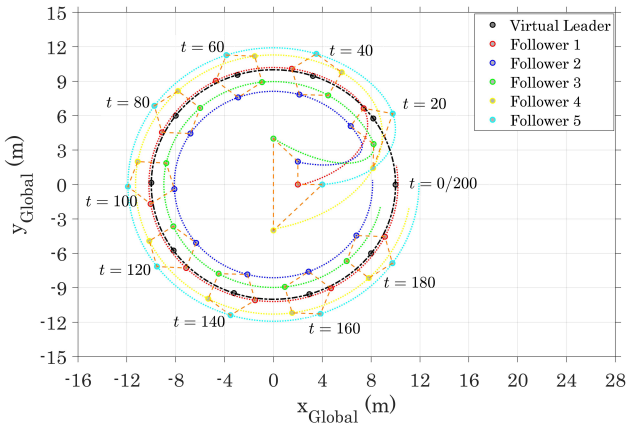

Fig. 10: Regular pentagonal formation ($R_f = 2$) of five differential-drive robots around the virtual leader

the virtual leader is assigned a reference trajectory given by $[x_d(t),\ y_d(t)] = [10\cos(2\pi t/T_{sim}),\ 10\sin(2\pi t/T_{sim})]$, where $T_{sim} = 200s$. The initial pose of virtual leader $[x_0^0,\ y_0^0,\ \theta_0^0] = [x_d(0),\ y_d(0), 1.57]$. The robots' initial poses and local angular positions (α_i) are given below.

$$\begin{bmatrix} x_1^0 & x_2^0 & x_3^0 & x_4^0 & x_5^0 \\ y_1^0 & y_2^0 & y_3^0 & y_4^0 & y_5^0 \\ \theta_1^0 & \theta_2^0 & \theta_3^0 & \theta_4^0 & \theta_5^0 \\ \alpha_1 & \alpha_2 & \alpha_3 & \alpha_4 & \alpha_5 \end{bmatrix} = \begin{bmatrix} 2 & 2 & 0 & 0 & 4 \\ 0 & 2 & 4 & -4 & 0 \\ 1 & -0.5 & 0 & -1 & 0 \\ 0 & 2\pi/5 & 4\pi/5 & 6\pi/5 & 8\pi/5 \end{bmatrix}$$

Results of example 2 are shown in Fig.10, which highlights a group of $N = 5$ robots converging to the desired formation around the virtual leader and the center of formation (coinciding with the virtual leader) tracking the reference trajectory.

Example 3: In this example, we consider a circular formation of $N = 4$ robots with $R_f = 4m$. The reference trajectory assigned to virtual leader is $[x_d(t),\ y_d(t)] = [10\cos(2\pi t/T_{sim}),\ 5\sin(2\pi t/T_{sim})]$, where $T_{sim} = 360s$. For the chosen reference trajectory, the value of $R_{des}^{min} = 2.5m$, $|v_{traj}^{sup}| = \pi/18 m/s$. Except $|v_{traj}^{sup}|$, control parameters listed in Table I are used. The initial pose of virtual leader $[x_0^0,\ y_0^0,\ \theta_0^0] = [x_d(0),\ y_d(0), 1.57]$. The local angular position (α_i) and initial pose of follower robots for this example are as follows

$$\begin{bmatrix} x_1^0 & x_2^0 & x_3^0 & x_4^0 \\ y_1^0 & y_2^0 & y_3^0 & y_4^0 \\ \theta_1^0 & \theta_2^0 & \theta_3^0 & \theta_4^0 \\ \alpha_1 & \alpha_2 & \alpha_3 & \alpha_4 \end{bmatrix} = \begin{bmatrix} 1 & 1 & 1 & 0 \\ 0 & 1 & -1 & -0.5 \\ 1 & -1 & 0 & -1 \\ 0 & \pi/2 & \pi & 3\pi/2 \end{bmatrix}$$

Fig.11 displays the simulation results of example 3. The robot closest to the center of curvature of the virtual leader's trajectory, i.e., Follower 2, undergoes sharp turns at $[-10,\ 0]$, $[10,\ 0]$. Disobeying condition in (38) caused violation of *Assumption* 1, resulting in breach of angular velocity limits in Follower 2, see Fig.12.

IV. Conclusion

In this work, we presented a novel control law for trajectory tracking control of multi-robot formation. Our proposed Lyapunov-based controller guarantees ultimate boundedness

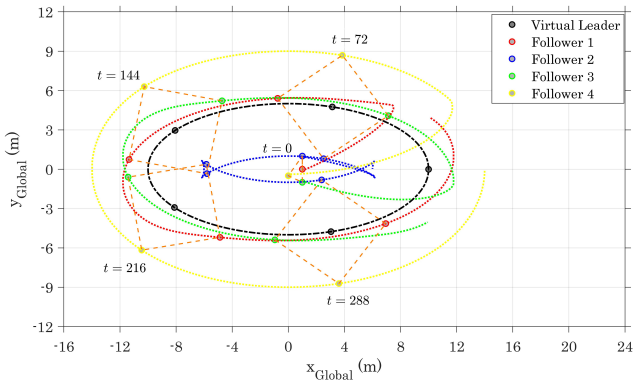

Fig. 11: Square formation ($R_f = 4m$) of four differential drive robots around the virtual leader

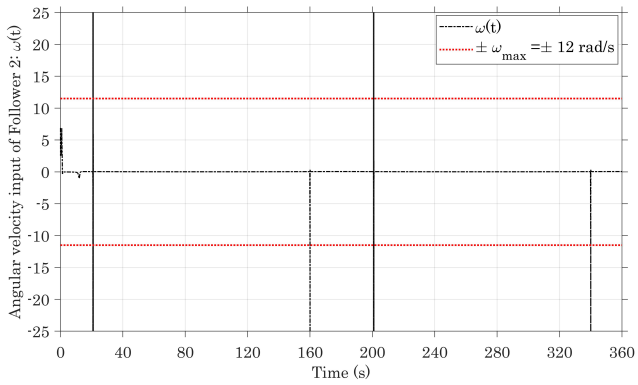

Fig. 12: Choice of $R_f = 4m > R^{des}_{min} = 2.5m$, violated assumption 4 resulting in $\omega(t) > \omega_{max}$ in Follower 2

on small tracking errors under input saturation for a single robot. The controller also ensured stability on being extended to trajectory tracking control of multi-robot formation in a virtual structure framework. We further discussed the impacts of large formation size on the kinematics of robots in a formation and hence proposed constraints on formation size to prevent instability and speed limit violations in robots. We believe practical input constraints are the key enablers in using the proposed controller in real deployments. However, additional work is necessary to ensure robust control under measurement, actuator, and plant uncertainties before considering practical deployments. We also plan to integrate CBF [19] with the proposed strategy to prevent collisions with static and moving objects. In addition to these topics, we will use a decentralized approach to formation control in our future work.

REFERENCES

[1] S. Mastellone, D. M. Stipanovic and M. W. Spong, "Remote Formation Control and Collision Avoidance for Multi-Agent Nonholonomic Systems," Proceedings 2007 IEEE International Conference on Robotics and Automation, 2007, pp. 1062-1067.

[2] C. B. Low, "A Flexible Leader-Follower Formation Tracking Control Design for Nonholonomic Tracked Mobile Robots with Low-Level Velocities Control Systems," 2015 IEEE 18^{th} International Conference on Intelligent Transportation Systems, 2015, pp. 2424-2431.

[3] Luca Consolini, Fabio Morbidi, Domenico Prattichizzo, Mario Tosques, "Leader–follower formation control of nonholonomic mobile robots with input constraints," Automatica, Volume 44, Issue 5, 2008, Pages 1343-1349.

[4] S. Xiao, L. Feng, H. Lian and B. Du, "Dynamic formation and obstacle avoidance control for multi robot system," 2016 12^{th} World Congress on Intelligent Control and Automation (WCICA), 2016, pp. 59-63.

[5] C. M. Elias, S. K. El-Baklish, N. N. El-Ghandoor, O. M. Shehata and E. I. Morgan, "Practical Hybrid Graph-Based Formation Control Architecture for Leader-Follower Trajectory Tracking Problem," 2018 IEEE International Conference on Vehicular Electronics and Safety (ICVES), 2018, pp. 1-6.

[6] L. Yan and B. Ma, "Practical Formation Tracking Control of Multiple Unicycle Robots," in IEEE Access, vol. 7, pp. 113417-113426, 2019.

[7] D. Kostić, S. Adinandra, J. Caarls, N. van de Wouw and H. Nijmeijer, "Saturated control of time-varying formations and trajectory tracking for unicycle multi-agent systems," 49th IEEE Conference on Decision and Control (CDC), Atlanta, GA, USA, 2010, pp. 4054-4059.

[8] H. Liang, C. Wang, H. Chen and X. Wu, "A synchronous approach to trajectory tracking in multirobot formation control with time delays," 2013 IEEE International Conference on Information and Automation (ICIA), 2013, pp. 671-676.

[9] R. Dongxu and Y. Shuanghe, "Trajectory tracking control of circular formation of agents with tracking different reference variables," 2015 34th Chinese Control Conference (CCC), 2015, pp. 7563-7568.

[10] Wei Ren, Nathan Sorensen, "Distributed coordination architecture for multi-robot formation control". Robotics and Autonomous Systems, Volume 56, Issue 4, 2008, pp. 324-333.

[11] W. Dong and J. A. Farrell, "Cooperative Control of Multiple Nonholonomic Mobile Agents," in IEEE Transactions on Automatic Control, vol. 53, no. 6, pp. 1434-1448, July 2008.

[12] K. Cao, Gao Xiang and Hongyong Yang, "Formation control of multiple nonholonomic mobile robots," International Conference on Information Science and Technology, 2011, pp. 1038-1042.

[13] T. Balch and R. C. Arkin, "Behavior-based formation control for multirobot teams," in IEEE Transactions on Robotics and Automation, vol. 14, no. 6, pp. 926-939, Dec. 1998.

[14] M. Zhang, Y. Shen, Q. Wang and Y. Wang, "Dynamic artificial potential field based multi-robot formation control," 2010 IEEE Instrumentation & Measurement Technology Conference Proceedings, 2010, pp. 1530-1534.

[15] K. Majd, M. Razeghi-Jahromi and A. Homaifar, "A stable analytical solution method for car-like robot trajectory tracking and optimization," in IEEE/CAA Journal of Automatica Sinica, vol. 7, no. 1, pp. 39-47, January 2020.

[16] Hassan K. Khalil, 2002, *Nonlinear Systems*, Prentice Hall, $3rd$ ed.

[17] Unwrap function, MATLAB Version (R2020a), The MathWorks, Inc., Natick, Massachusetts, United States. https://in.mathworks.com/help/matlab/ref/unwrap.html

[18] Agrawal, Ayush; Bharatheesha, Mukunda; Kolathaya, Shishir (2023): Formation control of differential-drive robots with input saturation and constraints on formation size. TechRxiv. Preprint. https://doi.org/10.36227/techrxiv.21984998

[19] A. D. Ames, S. Coogan, M. Egerstedt, G. Notomista, K. Sreenath and P. Tabuada, "Control Barrier Functions: Theory and Applications," 2019 18th European Control Conference (ECC), 2019, pp. 3420-3431.